SUPPLEMENTAL DATA

SUPPLEMENTAL METHODS

Subjects

The study was approved by the Essex 1 Research Ethics Committee (Ref no. 11/EE/0026) and the ARSAC (Administration of Radioactive Substances Advisory Committee). All subjects gave written informed consent and were given financial compensation for the time spent in their participation in the study. Healthy controls were recruited from a database of volunteers and patients with MS were referred by consultant neurologists. For healthy volunteers, exclusion criteria included any medical, neurological, or psychiatric illness at screening or any concomitant pharmacological treatments. All structural MRI images were inspected for unexpected findings of potential clinical significance or features that might confound PET co-registration or quantitative analysis by an experienced clinical neuroradiologist. Focal, non-specific alterations in the WM signal intensity were found in one healthy volunteer and the subject was referred for further evaluation. This volunteer had no past or present neurological symptoms and the physical and neurological examination was unremarkable. No other abnormalities were found. The neuroradiologist did not judge the findings to be clinically significant or to suggest pathology. This subject has been included in the analysis. Another healthy volunteer, who underwent two scans in consecutive days to assess ^{18}F-PBR111 PET reproducibility, had diffuse WM hyperintensities at MRI that were deemed compatible with the presence of cerebral small vessel disease. The subject was excluded from the between groups (MS vs. healthy controls) analyses, but was included in the analysis of the test-retest reproducibility of the signal.

All patients had relapsing-remitting MS based on neurological history and previous evaluations. The clinical and demographic characteristics of subjects, as well as the concomitant medications used, are listed in Supplemental Table 1. No subject received steroid treatment in the month before the PET scans and patients receiving disease-modifying treatments did not change in treatment for at least 3 months prior to scanning. In one MS patient (Supplemental Table 1, case 7) we found 2 Gd-enhancing lesions on T1-weighted MRI. No contrast enhancement was found in any of the other patients.

The EDSS and MSSS scores of one patient (Supplemental Table 1, case 1) were not considered in the analysis as most disability for the patient had been attributed previously to an incomplete traumatic spinal cord injury causing weakness in lower limbs, which was antecedent to the onset of MS.

Radioligand Synthesis

^{18}F-PBR111 was labelled with fluorine-18 by a simple one-step tosyloxy-for-fluorine nucleophilic aliphatic substitution, followed by purification by semi-preparative HPLC and reformulation. The synthetic procedure of ^{18}F-PBR111 was adapted from a previously described method (*1*). A fully automated procedure was developed in-house using a Siemens Explora GN module coupled with a semi-preparative HPLC system.

^{18}F-Fluoride, produced using a Siemens RDS-111 Eclipse cyclotron equipped with a fluoride target loaded with oxygen-18 enriched water, was obtained by means of the ^{18}O(p,n)^{18}F reaction. The ^{18}F-fluoride in solution in oxygen-18 enriched water was then trapped onto a DW-TRC-L trap and release cartridge (O.R.T.G.). Following that first step the fluoride was released into the reactor using 1.0 mL of a solution

consisting of 8.3 mL of acetonitrile, 0.8 mL of water, 250 mg of K_{222} and 50 mg of K_2CO_3. The content of the reactor was evaporated a first time and then the evaporation process was repeated 2 times following the addition of 1 mL of acetonitrile each time. The toxyloxy precursor (6.0-10.0 mg in solution in 1.0 mL of anhydrous acetonitrile) was then added to the reactor containing the "dry" [^{18}F]fluoride. The reaction mixture was heated for 5 min at 100 ºC and then cooled to 50 ºC before diluting with water. The crude reaction mixture was then diluted with water (3 ml) and loaded onto the HPLC injection loop for purification on an Agilent Eclipse XDB C18 column (5 µm, 250 × 9.4 mm) with ammonium formate buffer (pH 4)/CH_3CN (55:45, v/v) at 9.5 mL/min. The fraction containing ^{18}F-PBR111 was collected in water (20 ml) and loaded onto an activated Waters Sep-Pak® Classic C18 cartridge (Waters Corp.) for reformulation. Following an initial SepPak® column wash with water, ^{18}F-PBR111 was eluted off the column with ethanol and 0.9% saline solution for injection to lead to ^{18}F-PBR111 formulated in 11 mL of maximum 20% (v/v) ethanol in 0.9% saline solution for injection. In the final step a sterile filtration through a 0.2 µm sterile filter (Millipore Millex GV, 0.22 µm, 33 mm) was performed to deliver the final dose as a sterile and pyrogen-free solution.

Typically, the total ^{18}F-PBR111 synthesis procedure, including HPLC purification and Sep-Pak®-based formulation, was accomplished in less than 60 min. Up to 4.2 GBq of ^{18}F-PBR111 (>97% radiochemically pure, n>20) were obtained starting from 10 GBq of [^{18}F]fluoride with a specific radioactivity of up to 480 GBq/µmol.

MRI Protocol

T1-weighted (with and without Gd), T2-weighted FLAIR and MTR image sequences were acquired over a period of 60 minutes on a Siemens 3T Verio clinical MRI

scanner (Siemens Healthcare, Erlangen Germany) equipped with a 32-channel phased-array head coil. T1-weighted structural images for PET co-registration used the Alzheimer's Disease Neuroimaging Initiative (ADNI) recommended parameters with a parallel imaging factor of 2 in 5m:09s (*2*). T1-weighted images were acquired pre- and post- iv Gd-chelate administration (0.1 mmol/kg Gadoteric Acid, Dotarem®). Volumetric T2-weighted FLAIR images were acquired using a 1mm isotropic resolution 3D SPACE sequence (*3*), with a 250x250x160mm FOV, TE=395ms, TR=5s, TI=1800ms, turbo factor of 141, 256x256x160 matrix, and parallel imaging factor of 2 in 5m:52s. MTR maps were acquired using a 3D spoiled gradient echo sequence [fast low angle shot (FLASH)]. Two volumes with 1mm isotropic resolution were acquired using 256x240x192mm FOV, TR of 27ms and a flip angle of 5° to give pseudo proton density weighting (PDw), a parallel imaging factor of 2, 6 echoes acquired using 630Hz/pixel bandwidth with TEs every 1.95ms from 1.95 to 11.7ms in 7m:20s. Each high-bandwidth echo was summed to increase signal-to-noise ratio without introducing off-resonance effects of low readout bandwidth (*4*). One volume used a 12.24ms duration Gaussian RF pulse at 2.2 kHz off resonance with a nominal flip angle of 540° to add magnetization transfer weighting (MTw). MTR maps were calculated using the signals from the MTw and PDw acquisitions by the equation:

$$MTR = 100 \cdot (S_{PDw} - S_{MTw}) / S_{PDw} \qquad [1]$$

PET Protocol

Median injected ^{18}F-PBR111 mass was 0.33 μg (range 0.16 – 8.66) in healthy volunteers and 0.50 μg (range 0.2 – 1.9) in MS patients.

PET data were reconstructed using filtered back projection including corrections for attenuation and scatter (based on a low-dose CT acquisition). Dynamic data were binned into 29 frames (durations: 8 x 15 s, 3 x 1 min, 5 x 2 min, 5 x 5 min, 8 x 10 min).

Arterial blood data were sampled via the radial artery to enable generation of an arterial plasma input function. A continuous sampling system (ABSS Allogg, Mariefred, Sweden) was used to measure whole blood activity each second for the first 15 minutes of each scan. Discrete blood samples were manually withdrawn at 5, 10, 15, 20, 25, 30, 40, 50, 60, 70, 80, 90, 100, 110 and 120 minutes after scan start to facilitate measurement of whole blood and plasma activity. Samples taken at 5, 10, 15, 20, 30, 50, 70, 90 and 120 minute time points were also analysed using HPLC to determine the fraction of radioactivity corresponding to intact parent compound in arterial plasma. The first three discrete blood samples were used to calibrate the continuous blood data, and then the continuous and discrete data sets were used to form a whole blood activity curve covering the duration of the scan. Discrete plasma samples were divided by the corresponding whole blood samples to form plasma-over-blood (POB) data. A constant POB model was fitted (i.e. average of POB values). This POB value was then multiplied by the whole blood curve to generate a total plasma curve. Parent fraction data were fitted to a sigmoid model f= $((1-(t^3./(t^3+10^a)))^b+c)/(1+c)$ where t is time and a, b and c are fitted parameters. The resulting fitted parent fraction profile was multiplied by the total plasma curve and then smoothed post-peak using a tri-exponential fit to derive the required parent plasma input function. For each scan, a time delay was fitted and applied to the input function to account for any temporal delay between blood sample measurement and the tomographic measurements of the tissue data.

In three cases (Supplemental Table 1, cases n. 2, 3, 11), patients were not able to tolerate the whole duration of the scan due to increased discomfort related to neurological symptoms (i.e. muscular spasms and pain). In these cases we considered the V_T obtained from the analysis of the first 70 minutes of dynamic acquisition post injection. However, this is likely to lead to underestimation of V_T for these cases, as demonstrated by our previous analysis of time stability of V_T (Guo et al., 2013). Within subject comparisons of V_T obtained with acquisitions of 70 minutes vs 120 minutes in our sample indicated that scan duration of 70 min would lead to 7 to 35 % (median 16%) underestimation of V_T in comparison to values obtained from the full 120min acquisition. On the basis of these data, we applied a correction to the V_T of the 3 patients who could not complete the scan, increasing their V_T values of 16%.

Definition of Whole White Matter and T2-FLAIR Lesions

In healthy volunteers and MS patients, the whole WM was segmented automatically from each individual's structural T1 MRI image using SPM5 (Wellcome Trust Center for Neuroimaging, http://www.fil.ion.ucl.ac.uk/spm).

To define demyelinating lesions in MS patients' brains, T2- Fluid attenuated inversion recovery (FLAIR) hyperintense WM volumes were segmented using JIM version 6.0 (Xinapse Systems, Northants) by an experienced MRI analyst (NM) (Fig.1 a, b). The WM of patient, segmented using SPM5, was filled with T2 FLAIR lesions to complete the whole WM mask.

Statistical Analysis

All analyses were conducted using SPSS 20.

Between-Subjects Comparisons. ^{18}F-PBR111 V_T^{WM} was compared between binding affinity classes (HABs, MABs, LABs) by using non-parametric comparison for independent samples (Kruskal-Wallis Test). We compared ^{18}F-PBR111 V_T^{WM} of MS patients to that of healthy controls by using a two-tailed Wilcoxon Signed-Rank Test. Healthy volunteers' ^{18}F-PBR111 V_T^{WM} was compared to each of MS patients' VOI (V_T^{L}, V_T^{PL}, V_T^{NLLM}, V_T^{NLHM}) separately using two-tailed Wilcoxon Signed-Rank Tests. For those subjects (four healthy volunteers, and one MS patient) who underwent two scans in consecutive days, the mean ^{18}F-PBR111 V_T of the two visits for all VOIs have been used in all between- and within- subject analyses.

Within-Subjects Comparisons. Within MS patients, V_T^{L}, V_T^{PL}, and V_T^{NLLM} were separately compared to V_T^{NLHM}, by using two-tailed Wilcoxon Signed-Rank Tests. Significance for all tests was set at 0.05.

Correlations with Clinical Measures. The relationship between V_T^{WM} and disease duration was studied by means of Spearman's partial rank correlation. The partial rank correlation (ρ) coefficient was computed while correcting for the effect of age. We explored the relationship between disease severity and relative increase in TSPO density within demyelinating lesions, by studying the Spearman's rank coefficient of correlation (ρ) between MSSS score and Δ_L. For this analysis, we considered all T2-FLAIR lesions for each patient as a single VOI.

Partial Volume Correction. In order to estimate the partial volume effect on the outcome measure V_T, a voxel-region based algorithm for Partial Volume Correction (PVC), consisting in Local Regression Analysis (LoReAn) (*5*), has been applied as an exploratory tool to the PET brain volumes of one MS patient (case 9, Supplemental Table 1). ^{18}F-PBR111 V_T was estimated after PVC in the two largest lesional volumes and related perilesions, as well as in the NLHM WM area of the same patient. The relative increases in V_T in those two lesions and perilesional volumes vs NLHM, derived with and without PVC, were compared.

SUPPLEMENTAL RESULTS

Gd-Enhancing Lesions

The volume of the two Gd-enhancing lesions was 16 mm^3 (lesion 1) and 8 mm^3 (lesion 2) respectively. There was a 23% increase in ^{18}F-PBR111 V_T relative to NLHM volume in lesion 1, while in lesion 2 there was no change in ^{18}F-PBR111 V_T relative to NLHM volume. In perilesional volumes, the increase in ^{18}F-PBR111 V_T relative to NLHM volume was 10 % and 1 %, for lesion 1 and lesion 2 respectively. The volume of these lesions was very small, especially for lesion 2 where the volume corresponded to only one voxel in a 2x2x2mm space.

Partial Volume Correction

The relative increase in ^{18}F-PBR111 V_T in the two lesions (case no. 9, Supplemental Table 1) examined after PVC were higher than pre-PVC (post-PVC Δ_L, 59.8% and 102.5%; pre-PVC Δ_L, 34.7% and 40.7%, respectively). The relative increase in ^{18}F-

PBR111 V_T vs NLHM in perilesional volumes was not meaningfully altered by PVC (post-PVC Δ_{PL}, 18.9 % and 17.5%; pre-PVC Δ_{PL}: 17.9% and 20.8%, respectively).

SUPPLEMENTAL DISCUSSION

We found considerable variability in ^{18}F-PBR111 V_T between subjects, independent of their TSPO genotypes. The positive correlation between age and binding may explain some of this (*6*), but other factors also must contribute. The assessment of test-retest reproducibility of V_T demonstrated moderate measurement variance. One contribution to this can arise from identification of the true parent plasma input function. TSPO is abundant in the body and blood. Variation in the proportions of any displaceable (specific) and non-displaceable (non-specific) binding signals in plasma and tissue can also lead to variability. Consistent with these hypotheses, we found that the test-retest reproducibility of lesional and perilesional signal in MS was significantly improved after normalization by correction for normal-appearing WM signal with normal MTR. Normalization of focal signal intensity in T2-MRI lesions by correction for NLHM values may be a particularly useful approach for increased precision of assessments in longitudinal studies.

The extent of inter-subject variability despite correction for genotype and the relatively large overlap of ^{18}F-PBR111 signal between control and patient populations are consistent with data obtained with other 2nd generation TSPO radioligands in MS and other neuroinflammatory diseases (*7*-*9*). These may indicate that clinical applications of TSPO PET imaging will require large sample sizes to detect increases in microglia activation in patient populations. In longitudinal applications, the use of normalisation (as suggested above) would reduce test-retest variability,

increasing precision of the assessments, but may potentially lead to underestimation of changes in binding over time. All together these are limitations that may blunt the sensitivity of TSPO PET for detection of neuroinflammatory processes in vivo.

A number of methodological aspects are worth considering. Partial volume effect may have confounded accurate measurement of binding and led to the underestimation of increases of TSPO binding in lesional ROIs. This should influence estimates in smaller regions to the greatest extent, but we have found no evidence in Bland-Altman plots that smaller volumes were associated to lower increases, suggesting that this was not a dominant effect (data not shown). Furthermore, PVC applied to two large lesional volumes as an exploratory tool, suggested that tissue differences may be underestimated due to volume averaging. In fact, the relative increase in ^{18}F-PBR111 uptake in lesions was enhanced after PVC. However, as PVC did not affect the relative increases in perilesional volumes, it is unlikely that our observation of increased TSPO uptake in perilesional white matter was artifactually confounded by partial volume effects.

As ^{18}F-PBR111 V_T reflects both displaceable (presumed specific for TSPO) and non-displaceable (non-specific or off-target binding) binding, the true differences in inflammatory response between VOIs may be underestimated. We estimate that the proportion of ^{18}F-PBR111 V_T corresponding to specific signal ranges between 30 and 70% across genotypically defined binding affinity classes (Guo et al., 2013). The observed increases in lesion associated signal (ranging between 15 - 50% relative to the normal-appearing tissue) therefore suggest an increase in microglia-related TSPO binding of between 20 - 80% across different lesions.

While a 2-tissue compartment model has been found to fit the data well, we have

observed that V_T increases slightly with time for reasons not yet well understood (*6*). This could have been due to some small, irreversible contribution, e.g., from slow entry of a radio-labelled metabolite into the CNS and its non-specific association. We attempted to control for this in our analysis by applying a correction factor to the values obtained with shorter scan durations intended to minimize biases due to underestimation of the signal. If the statistical analysis were run without the three subjects with shorter scan duration, we would have observed significant higher V_T in all MS patients' ROIs (including NLHM and NLLM) relative to healthy controls V_T^{WM} (all $p<0.05$). The correlation between MSSS severity and ^{18}F-PBR111 V_T increase in lesions would have remained significant ($r=0.76$; $p<0.05$) while the partial correlation between disease duration and V_T^{WM} in HABs would have lost significance ($r=0.88$; $p=0.12$); however, only 5 subjects would have been left for this analysis.

Finally, it is worth mentioning that two MS patients were on natalizumab treatment at the time of the ^{18}F-PBR111 scan (Supplemental Table 1). Natalizumab treatment reduces the relapse rate in MS patients more effectively than other available treatments (*10, 11*). We hypothesize that treatment with natalizumab in those two patients may have reduced ^{18}F-PBR111 binding to a greater extent than was apparent in other patients treated with interferon-β, however further research is necessary to differentiate the effects on TSPO specific binding of specific disease-modifying treatments for MS.

SUPPLEMENTAL REFERENCES

1. Fookes CJ, Pham TQ, Mattner F, et al. Synthesis and biological evaluation of substituted [18F]imidazo[1,2-a]pyridines and [18F]pyrazolo[1,5-a]pyrimidines for the study of the peripheral benzodiazepine receptor using positron emission tomography. *J Med Chem.* 2008;51:3700-3712.

2. Jack CR, Jr., Bernstein MA, Fox NC, et al. The Alzheimer's Disease Neuroimaging Initiative (ADNI): MRI methods. *J Magn Reson Imaging.* 2008;27:685-691.

3. Mugler JP, Brookeman JR. Ultra-long echo trains for rapid 3D T2-weighted turbo-spin-echo imaging. *Proceedings of the 11th International Society of Magnetic Resonance in Medicine.* 2003:970.

4. Helms G, Dechent P. Increased SNR and reduced distortions by averaging multiple gradient echo signals in 3D FLASH imaging of the human brain at 3T. *Journal of Magnetic Resonance Imaging.* 2009;29:198-204.

5. Coello C, Willoch F, Selnes P, Gjerstad L, Fladby T, Skretting A. Correction of partial volume effect in (18)F-FDG PET brain studies using coregistered MR volumes: Voxel based analysis of tracer uptake in the white matter. *Neuroimage.* 2013;72:183-192.

6. Guo Q, Colasanti A, Owen DR, et al. Quantification of the specific translocator protein signal of [18F]PBR111 in healthy humans: a genetic polymorphism effect on in vivo binding. *J Nucl Med.* 2013;54:1915-1923.

7. Kreisl WC, Lyoo CH, McGwier M, et al. In vivo radioligand binding to translocator protein correlates with severity of Alzheimer's disease. *Brain.* 2013;136:2228-2238.

8. Oh U, Fujita M, Ikonomidou VN, et al. Translocator protein PET imaging for glial activation in multiple sclerosis. *J Neuroimmune Pharmacol.* 2011;6:354-361.

9. Takano A, Piehl F, Hillert J, et al. In vivo TSPO imaging in patients with multiple sclerosis: a brain PET study with [18F]FEDAA1106. *EJNMMI Res.* 2013;3:30.

10. Mellergard J, Edstrom M, Vrethem M, Ernerudh J, Dahle C. Natalizumab treatment in multiple sclerosis: marked decline of chemokines and cytokines in cerebrospinal fluid. *Mult Scler.* 2010;16:208-217.

11. Stuve O, Bennett JL. Pharmacological properties, toxicology and scientific rationale for the use of natalizumab (Tysabri) in inflammatory diseases. *CNS Drug Rev.* 2007;13:79-95.

Supplemental Table 1

	Healthy Volunteers[a]			Relapsing-Remitting MS patients						
Case	binding affinity class	Age	Gender	binding affinity class	Age	Gender	EDSS	Disease Duration	MSSS	DMT
1	HAB	52	F	HAB	48	F	-	8	-	natalizumab
2	LAB	51	M	LAB	39	F	4	20	3.0	interferon β
3	HAB	42	F	HAB	40	F	4	11	4.9	natalizumab
4	HAB	59	M	HAB	55	F	2	20	0.9	interferon β
5	LAB	65	M	LAB	53	F	7	20	7.4	-
6	MAB	57	M	MAB	59	F	3	16	2.6	interferon β
7	HAB[b]	28	M	HAB	41	F	2.5	14	2.3	-
8	HAB[b]	28	M	HAB[b]	28	M	2	7	3.2	-
9	MAB	36	F	MAB	41	F	6	4	9.1	interferon β
10	HAB	33	F	HAB	42	F	6	1.5	9.6	interferon β
11	HAB[b]	52	F	HAB	50	F	4	2	8.6	interferon β
Mean age		45.7			45.1					

Supplemental Table 1. Demographic variables, TSPO binding affinity class, and clinical characteristics of study participants.

EDSS: Expanded Disability Status Scale; MSSS: Multiple Sclerosis Severity Score; DMT: Disease Modifying Treatment; HAB: High Affinity Binder; MAB: Mixed Affinity Binder; LAB: Low Affinity Binder.

[a] a twelfth healthy volunteer (genotype, HAB; age: 50 y.; gender: female) was included in the test-retest analysis but was excluded from the comparison between-groups due to white matter abnormalities consistent with presence of cerebral small vessel disease (see Subjects section). **[b]** These subjects underwent two scans in consecutive days to assess test-retest reproducibility.

Supplemental Figure 1

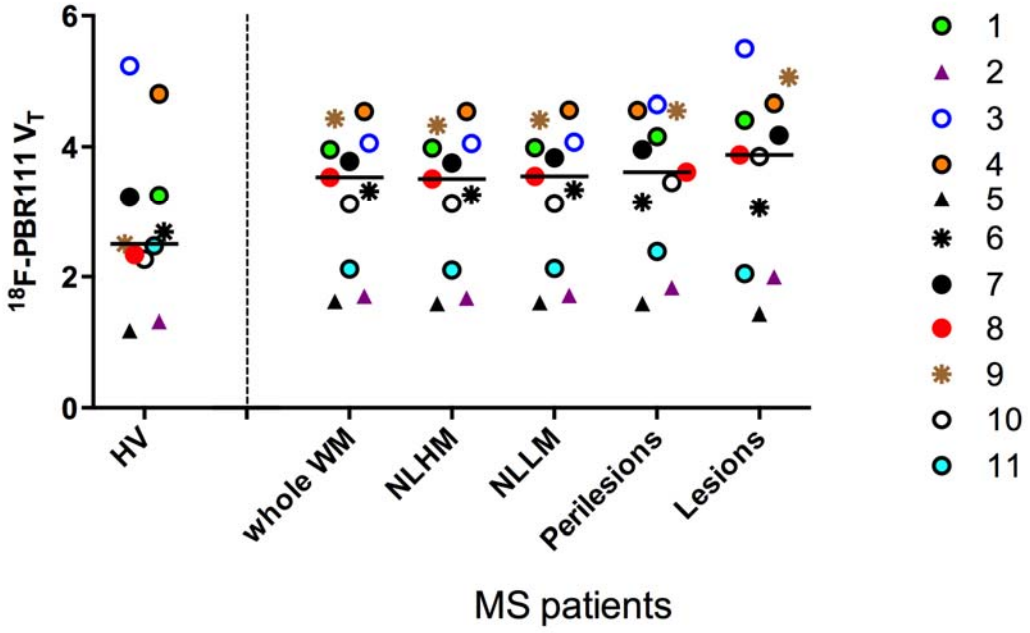

Supplemental Figure 1. Individual ^{18}F-PBR111 uptake in healthy volunteers and across MS patients ROIs.

Symbols represent separate subjects. For lesional and perilesional VOIs, each symbol represents the mean ^{18}F-PBR111 uptake for each patient across all lesions and perilesional volumes, respectively. In the legend, each symbol is numbered according to the cases' numbers listed in Supplemental Table 1. The shapes of the symbols indicate the binding affinity classes: triangles for LABs, stars for MABs, and circles for HABs.